Transportation Infrastructure Geotechnology (2024) 11:22–43
https://doi.org/10.1007/s40515-022-00270-2

TECHNICAL PAPER

Numerical Estimation of Bearing Capacity of Conical Footing Embedded in Sand

Vishwas Nandkishor Khatri[1] · Jitendra Singh Yadav[2,3] · Ketan Shrivastava[1]

Accepted: 1 December 2022 / Published online: 23 December 2022

Abstract
The present study demonstrates the computational bearing capacity estimation of conical footings resting on sand deposits. The parameters varied in this study were (i) embedment ratio, D_f/B (where: D_f=embedment depth of footing and B=diameter of footing) (0, 0.25, 0.5, 0.75, and 1), (ii) apex angle of conical footing, β (30°, 60°, 90°, 120°, 150°, and 180°), and (iii) friction angle of sand, ϕ (25°, 30°, 35°, 40°, and 45°). The Mohr–Coulomb failure criterion and the non-associated flow rule ($\psi<\phi$) were considered to be applicable to the soil. The results are expressed in terms of bearing capacity ratio (BCR) and settlement reduction factor (SRF). It is observed that for $\phi<30°$, the magnitude of bearing capacity decreases continuously with an increase in β from 30 to 180°. Whereas, for $\phi>30°$, the minimum bearing load capacity is found to occur generally between $\beta=120°$ and $\beta=150°$. In all the cases, it is noticed that the bearing capacity becomes maximum for $\beta=30°$. The bearing capacity values obtained are found comparable to those published in the literature.

Keywords Finite element analysis · Non-associated flow rule · Conical footing · Bearing Capacity ratio · Settlement reduction ratio

1 Introduction

The foundation is an essential component of the structures as it supports and transfers loads from the superstructure to the underlying soil. A well-built base spreads the loads from the superstructure in such a way that the underlying soil is not highly

✉ Jitendra Singh Yadav
Jitendershine@gmail.com

[1] Department of Civil Engineering, Indian Institute of Technology (ISM), Dhanbad, India

[2] Department of Civil Engineering, National Institute of Technology, Hamirpur, Himachal Pradesh, India

[3] Department of Civil Engineering, National Institute of Technology, Kurukshetra, Haryana, India

stressed. The overburdening of soil may result in the settlement of structure or shear failure of the soil. The bearing capacity of the soil is the amount of pressure at which the supporting soil is anticipated to fail in shear. The bearing capacity can be calculated using analytical methods or experimental studies. In recent years, several investigations have been performed on determining the bearing capacity factor N_γ for the strip, circular and conical footings. Conical footings represent spudcan foundations which are generally employed for different offshore structures. Cassidy and Houlsby (2002) provided the solution for finding the load-carrying capacity factors for smooth and rough conical footings resting on the surface of sand following the method of characteristics. In their study, sand friction angles were kept between 5 and 50°, while cone apex angles ranged between 30 and 180°. Lyamin et al. (2007) calculated the bearing capacity of strip, square, circular, and rectangular foundations in sand using finite-element limit analysis for frictional soils following an associated flow rule. Based on analytical results, shape, and depth factors were proposed to determine the bearing capacity of foundations embedded in the sand. Khatri and Kumar (2009) examined the effect of the apex angle β of the conical footing on the bearing capacity factor N_γ by varying the friction angle (ϕ) of sand, obeying an associated flow rule. The influence of β on the plastic zones was also investigated. In another study, Kumar and Khatri (2011) used the lower bound limit analysis in conjunction with finite element and linear programming to calculate the bearing capacity factors for a circular footing due to cohesion, surcharge, and unit weight with various values of ϕ. Chakraborty and Kumar (2015) estimated the bearing capacity factors, N_c, N_q, and N_γ, for numerous combinations of β, ϕ, and δ, using the lower and upper bound axisymmetric formulation of limit analysis combined with finite elements and linear optimization. The variations of N_c, N_q, and N_γ in a bound form for various combinations of ϕ and δ were illustrated and compared to Houlsby and Martin's stress characteristic solution (Houlsby and Martin 2003). Furthermore, Chakraborty and Kumar (2016) explored the dependence of N_c on footing diameter for a conical foundation utilizing limit analysis in combination with finite elements and linear programming for different cone apex angles. The investigation was carried out using two well-defined ϕ versus σ_m curves from the literature. According to the analysis, the magnitude of N_γ diminishes with the increase in footing diameter (B) for all cone apex angles. For a rough footing, the decrease of N_γ with an increase in B becomes more widespread. With B greater than 0.45 m approximately for a smooth footing and 0.85 m for a rough footing, the factor N_γ diminishes almost linearly with an increase in B on a log–log scale for which a simplified expression was generated relating N_γ and B. The reduction in N_γ with an increase in B becomes minimal for B bigger than about 8.0 m.

Keawsawasvong (2021a) proposed a novel plastic solution of the bearing capacity factor for conical footings on clays with linearly increasing anisotropic shear strength. With the increase in strength gradient ratio or anisotropic strength ratio, an increase in the bearing capacity factor was reported. But, with the increase in cone apex angle reduction in bearing capacity factor was observed. In another study, Keawsawasvong (2021b) proposed new plastic solutions for the bearing capacity factors of conical footings on rock masses obeying the Hoek–Brown yield criterion. A conical footing was penetrated into a rock mass. The effect of the cone apex angle, the yield parameter, and the geological strength index of a rock mass on the bearing capacity factors were evaluated. Lai et al. (2022) evaluated the bearing capacity of conical footings embedded in anisotropic and inhomogeneous clays using the NGI-ADP model. The bearing capacity factor of conical footings was defined as function of cone apex angle, strength gradient ratio, and anisotropic shear strength ratio. Phuor et al. (2022) computed of the vertical bearing capacity factors a rough conical footing placed on the soil with friction angle ranging from $\phi = 5$ to 45° by using the FE-based viscoplastic strain method under the Mohr–Coulomb (MC) yield criterion. It was observed that numerical stability with a high value of friction angle could be improved to some extent by employing the proper values of soil dilation angle. The bearing capacity factors were slightly decreased with the increase of the cone apex angle $\beta = 60°$ to $\beta = 180°$. However, considerable increment in bearing capacity factors was reported with the decrease of $\beta = 60°$ to $\beta = 30°$. Hu et al. (2022) investigated the horizontal bearing capacity factors for conical footing on clay, taking the effects of embedment ratio, foundation–soil interface roughness, conical angle, and soil strength heterogeneity in the account. At a specific embedment, an increment in horizontal bearing capacity factors was reported with strength gradient ratio, but with the increase in cone apex angle, decrement in bearing capacity factors was seen. The roughness factor had the least effect on the bearing capacity factors.

In the past, very little literature has been available on the bearing capacity of rough conical shallow footing resting on the sand. The shallow conical footing laying on the sand at various embedment ratios has not been examined thoroughly, utilizing different friction angles, and cone apex angles.

The present study uses the finite element method to determine the collapse loads for conical footings placed on the sand. The bearing capacity values were determined for various combinations of friction angles (ϕ) and cone apex angles (β) with different embedment ratios. The results obtained from the analysis were compared with those available in the literature.

2 Methodology

In the finite element method, the solution usually refers to the determination of the displacements at each node and the stresses inside each element in the structure subjected to the applied loads. The bearing capacity of a conical foundation lying on the sand was calculated using the finite element methods employing Optum G2. (2019) using the method suggested by Khatri et al. (2022). The footing was modeled with this software using the six-noded triangular gauss element and dividing the whole domain into 10,000 elements. The axisymmetric analysis was performed by utilizing a typical domain in the r-z plane.

During the analysis for conical footing, the axisymmetric condition was considered. The cylindrical coordinates are adopted with r, z, and θ representing radial, vertical, and circumferential directions. There are four non-zero stresses (σ_r, σ_z, σ_θ, and τ_{rz}), four non-zero strains (ε_r, ε_z, ε_θ, and Υ_{rz}), and two displacements ($\tilde{u}$ and w') in the r and z-direction, respectively. There is no displacement in the θ direction owing to the symmetry. The displacements in the r and the z

directions are independent of θ. Thus the strains and stresses are reduced to as shown in Eqs. (1) and (2), respectively.

$$\gamma r\theta = \gamma z\theta = 0 \tag{1}$$

$$\tau r\theta = \tau z\theta = 0 \tag{2}$$

The strain–displacement relationships are as follows:

$$\varepsilon r = \frac{\partial u'}{\partial r'},\ \ \varepsilon z = \frac{\partial w'}{\partial z'},\ \ \varepsilon\theta = \frac{\widetilde{u}}{r'},\ \gamma rz = \frac{\partial w'}{\partial r'} + \frac{\partial\widetilde{u}}{\partial z} \tag{3}$$

Every two-dimensional axisymmetric problem was required to satisfy the equilibrium stresses given by Eq. (3) and Eq. (5).

$$\frac{\partial\sigma r}{\partial r} + \frac{\partial\tau rz}{\partial z} + \frac{(\sigma r - \sigma\theta)}{r} = 0 \tag{4}$$

$$\frac{\partial\tau rz}{\partial r} + \frac{\partial\sigma z}{\partial z} + \frac{\tau rz}{r} = \gamma \tag{5}$$

Equations (1–5) can be used for the creation of the stiffness matrix, with the use of shape function for a six-noded triangular element and the relevant constitutive relationships (Potts et al. 2001).

The soil was modelled assuming as Mohr–Coulomb material and followed the non-associated flow rule. The soil domain was discretized using six noded finite triangular elements (linear strain triangle LST), with nodal displacements as unknown variables. The differential equation, strain compatibility equation, and boundary conditions for plane strain and axisymmetric analysis are already reported in Khatri et al. (2022). The strip footing follows the plain-strain condition during its analysis, wherein the strains and stresses considered are given by Eqs. (6) and (7), respectively. Here, the x, y, and z represent the three directions in the cartesian coordinate system, and u' and v' implies the displacements in the x and y directions. ε_x, ε_y, and ε_z are known as the longitudinal strains in the x, y, and z directions, respectively, whereas Υ is called the shear strain. Similarly, σ and τ represent normal and shear stresses.

$$\varepsilon z = \gamma xz = \gamma yz = 0 \tag{6}$$

$$\tau xz = \tau yz = 0, but\sigma z \neq 0 \tag{7}$$

Furthermore, the strain–displacement relationships for the plane-strain condition are as follows:

$$\varepsilon x = \frac{\partial u^{'}}{\partial x^{'}}, \varepsilon y = \frac{\partial v^{'}}{\partial y^{'}}, \gamma xy = \frac{\partial u^{'}}{\partial y^{'}} + \frac{\partial v^{'}}{\partial x^{'}} \tag{8}$$

The basic differential equations to satisfy plane strain conditions are given by Eqs. (9) and (10), where the parameter ν represents the Poisson's ratio.

$$\frac{\partial^2 u'}{\partial x^2} + \frac{\partial^2 u'}{\partial y^2} = \frac{1+\nu}{2}\left(\frac{\partial^2 u'}{\partial y^2} - \frac{\partial^2 v'}{\partial x \partial y}\right) \tag{9}$$

$$\frac{\partial^2 v'}{\partial x^2} + \frac{\partial^2 v'}{\partial y^2} = \frac{1+\nu}{2}\left(\frac{\partial^2 v'}{\partial x^2} - \frac{\partial^2 u'}{\partial x \partial y}\right) \tag{10}$$

It is pertinent to note that an additional plane strain analysis for strip footing is performed herein to determine shape and depth factors for conical footing in line, similar to Lyamin et al. (2007).

3 Problem Domain, Mesh Details, and Material Properties

Optum G2 software was used to conduct this numerical-based analysis. In this regard, the details regarding the problem domain, mesh, material properties used, and methodology are described in the following sections.

3.1 Problem Domain

For the sake of presentation, a rough conical footing embedded in the soil domain (represented by ABCE) is shown in Fig. 1, where the load (Q) acts in the downward direction. The horizontal displacement (u) along the line of symmetry (line "AB" in figure) and far-off boundary (line "CE" in figure) was kept at zero. In contrast, along the bottom boundary "BC," the horizontal displacement (u) and vertical displacement (w) were stated as zero. The parameter B, the diameter of the conical footing, was taken as 2 m. The parameter "*t*" means the thickness of the footing, which was taken as 0.25 m. L and V denote the length and depth of the selected domain. The values of L and V were computationally arrived at by using several trials like (i) the limits of the plastic zones fall well within the boundaries of the specified problem domain, and (ii) the magnitude of the collapse load remains almost constant even if the domain size was increased further. Approximately the L and V values were kept equal to 5B. No movement was enabled in either the vertical direction (w) or the horizontal direction (u) at the horizontal bottom of the selected domain. A six-noded element was used to model the soil and the footings.

3.2 Mesh Details

The whole domain was discretized into the number of elements resulting in meshes. In a given mesh, finer elements accumulate in a region wherein shear failure is evident. The meshes are generated for conical footing with different D_f/B values for various β. At $\phi = 40°$, the mesh details for conical footing at $D_f/B = 0$ and 1 with $\beta = 30°$, $\beta = 90°$ and $\beta = 180°$ is shown in Fig. 2. Note that the adaptive finite element

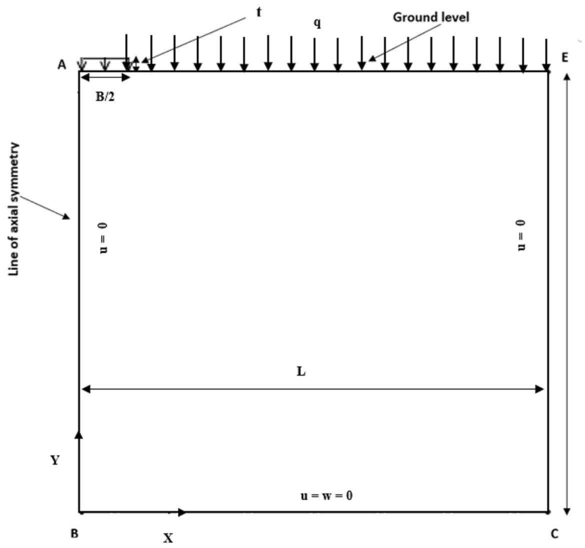

Fig. 1 Line diagram of conical footing embedded in the soil

meshes with a zone of finer elements shown in Fig. 2 indirectly reflect the failure patterns.

3.3 Material Properties

The properties of the material used in this analysis are as per Das et al. (2022). The properties of footing are listed in Table 1. The Modulus of elasticity of footing is calculated by E(MPa) = $5000\times(f_{ck})^{0.5}$, where f_{ck} is the characteristic compressive strength of concrete, and in the present study, it was taken as 20 N/mm^2.

The soil is assumed to be elastoplastic and follows the Mohr–Coulomb failure criterion and the non-associated flow rule ($\psi<\phi$). Furthermore, the dilation angle was taken as $\psi=(\phi\text{-}30°)$. The properties of sand are listed in Table 2 (Bowles 1996).

4 Results and Discussion

The finite element analysis was conducted for conical footing lying on the sand, obeying the non-associated flow rule for various depth ratios (D_f/B). The friction angle of sand is varied from 25 to 45°. In each case, the bearing capacity was estimated from the pressure-settlement curves. Furthermore, the bearing capacity was articulated using a non-dimensional parameter termed the bearing capacity ratio (BCR), which is a ratio of the bearing capacity of the conical footing to the bearing capacity of the circular footing. The BCR was calculated for two different scenarios: (1) at failure (BCR_u) and (2) at the settlement of 10% (BCR_{10}). Note that the term BCR signifies the bearing capacity improvement brought out with the use of conical footing instead of the circular footing of a similar diameter. A reduction in settlement with the use of conical footing in place of circular

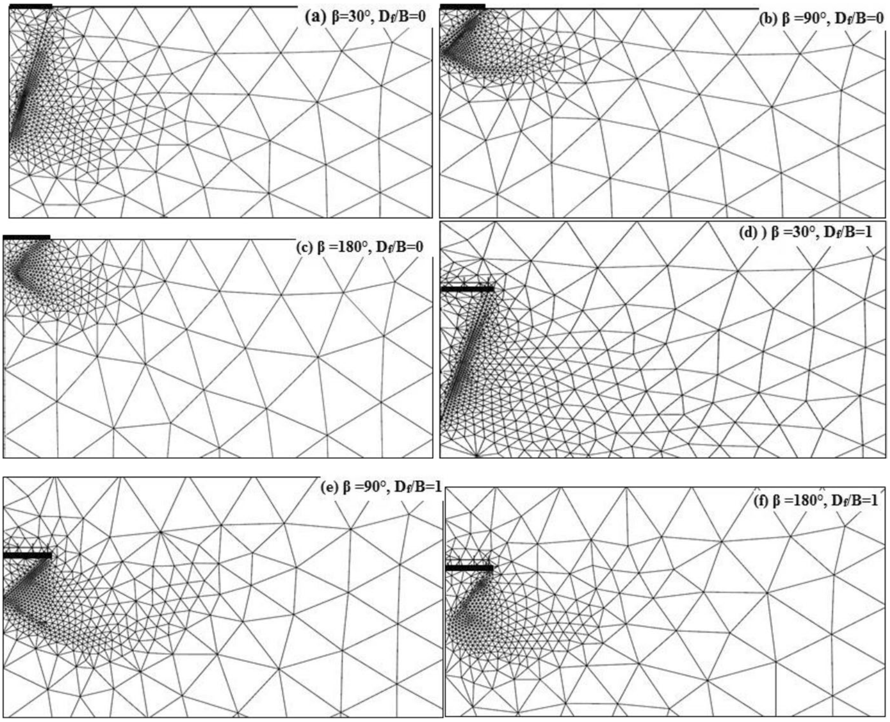

Fig. 2 Mesh details for conical footing at ϕ = 40°

Table 1 Properties of footing (Das et al. 2022)

Material of Footing	Modulus of elasticity (E)	Poisson's ratio (ν)	Unit weight (γ)
Linear elastic	22,360.68	0.2	24

Table 2 Properties of sand (Bowles 1996)

Soil consistency	Friction angle (ϕ)	Dilation angle (Ψ)	Elastic modulus (E) (MPa)	Poisson's ratio (μ)	Unit weight (γ) (kN/m^3)
Very loose sand	25°	5°	7	0.2	12
Loose sand	30°	5°	20	0.2	13.5
Medium sand	35°	5°	35	0.25	15.5
Dense sand	40°	10°	52	0.3	17.5
Very dense sand	45°	15°	75	0.35	20

footing at a given pressure was arrived at in terms of a settlement reduction factor (SRF), defined in the subsequent section. Like BCR, SRF has been defined as corresponding to the pressure at failure and S/D = 10% of circular footing and termed as SRF_u and SRF_{10}, respectively. The variations of all the above parameters are explained in subsequent sections.

4.1 Pressure-settlement variation

Figure 3(a)–(i) illustrate the variation of normalized pressure with normalized settlement for conical foundation resting over sand for different ϕ with $\beta = 30°$, 90°, and 180° at $D_f/B = 0$, 0.5, and 1. A normalized or equivalent pressure is found by fractioning the load-carrying capacity of the footing by (γB) and normalized settlement (S/D) is calculated by fractioning the settlement with the diameter of the footing (D). From the obtained plots, it can be observed that the bearing pressure for a given friction angle decreases on increasing apex angle. Also, the bearing pressure increases on increasing embedment depths. The ultimate bearing capacity of footing was determined using the pressure settlement plots using a double tangent method (Khatri et al. 2022). Additionally, the bearing pressure corresponding to S/D = 10% was determined. Using the magnitude of ultimate bearing capacity and bearing pressure corresponding to S/D = 10%, the terms BCR_u and BCR_{10} were computed as defined earlier.

4.2 Variation of BCR_u and BCR_{10} with β, D_f/B and ϕ

Figures 4 and 5, respectively, show the variation of BCR_u and BCR_{10} for various β and ϕ with $D_f/B = 0$, 0.5, and 1. It is worth noting that the bearing capacity decreases on increasing the cone's apex angle (β). The bearing capacity of conical footing is maximum at $\beta = 30°$. Accordingly, the BCR_u and BCR_{10} are maximum at $\beta = 30°$. For $\beta = 30°$, bearing capacity improvement at failure (BCR_u) over circular footing is in the range of 1.25 to 4.5, considering all the friction angles and embedment ratios. In contrast, the bearing capacity improvement corresponding to S/D = 10% (BCR_{10}) ranges from 1.15 to 3.25.

A close observation of Figs. 4 and 5 suggests that the BCR_u and BCR_{10} are maximum for a lower value of friction angle for surface footing (Df/D = 0). However, with an increase in embedment ratio, the trend is reversed. It can be reasoned that in the case of surface footing, a significant improvement is brought out in bearing capacity by changing the type of footing from circular (β= 180°) to conical (β= 30°) alone. However, as embedment depth increases, the bearing capacity improves due to soil shear strength above the base level of the foundation overweighing the change in footing type. Accordingly, the BCR_u and $BCR_{10,}$ in the case of embedded footing ($Df/D > 0$), were higher for a greater friction angle in contrast to the surface footing. Using Figs. 4 and 5, one can select a conical footing of the appropriate apex angle over a circular footing if an improvement in bearing capacity is desired, while friction angle and embedment depth are held constant.

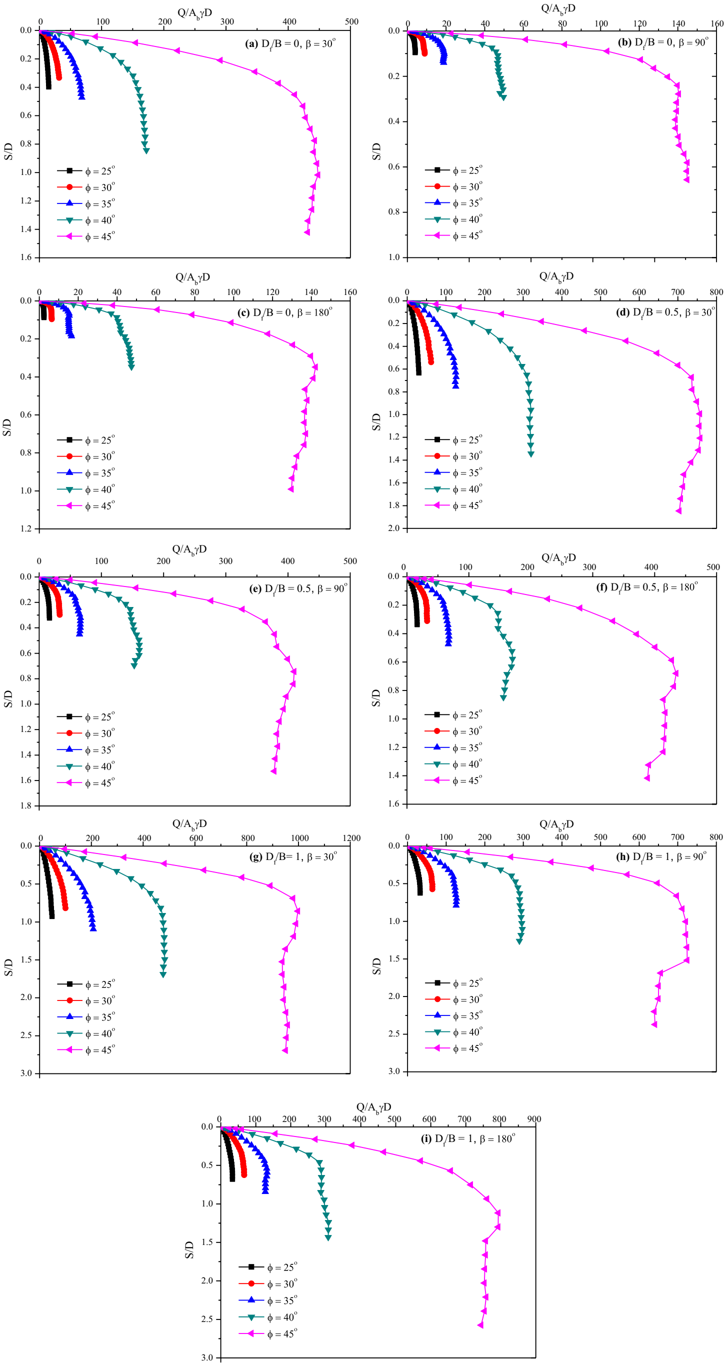

Fig. 3 Variation of $Q/(A_b\gamma D)$ with S/D (%) for different ϕ with $\beta = 30°$, 90°, and 180° at $D_f/B = 0$, 0.5, and 1

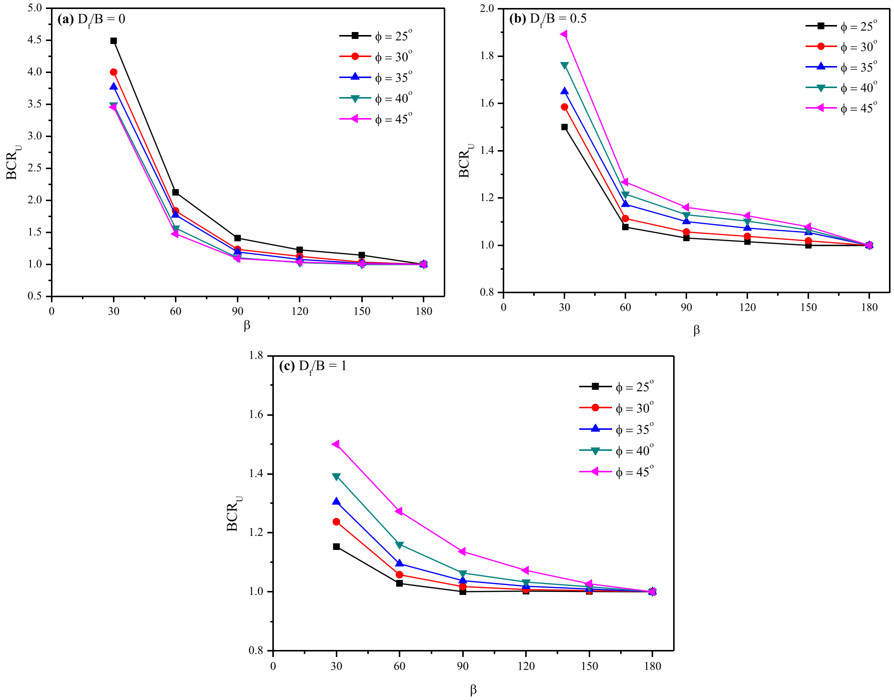

Fig. 4 Variation of bearing capacity ratio for different β and different ϕ with **a** $D_f/B = 0$, **b** $D_f/B = 0.5$, **c** $D_f/B = 1$

4.3 Variation of SRF at Failure and SRF at 10% Settlement with β at DifferentEmbedment Ratios for ϕ

SRF (settlement reduction factor) is defined as the fraction of the difference in the settlement between the conical footing and the circular footing to the settlement of the circular footing defined at a given pressure. Numerically the SRF is calculated by -:

$$SRF = \left[\frac{\left(\frac{S}{B}\right)_{\text{circular}} - \left(\frac{S}{B}\right)_{\text{conical}}}{\left(\frac{S}{B}\right)_{\text{circular}}} \right] \times 100 \tag{11}$$

The present study defines the SRF as corresponding to pressure i) at failure state (SRF_u) and ii) S/D = 10% (SRF_{10}) of circular footing. Figure 6a and b show the variation of SRF_u with β at failure for different ϕ at $D_f/B = 0$ and 1, respectively. It can be observed that SRF_u decreases on increasing apex angle. It implies that compared to circular footing, the conical footing is more efficient in settlement reduction apart from improvement in bearing capacity. As shown in Fig. 6a, the maximum reduction in settlement for a conical footing with a given apex angle was seen for the footing

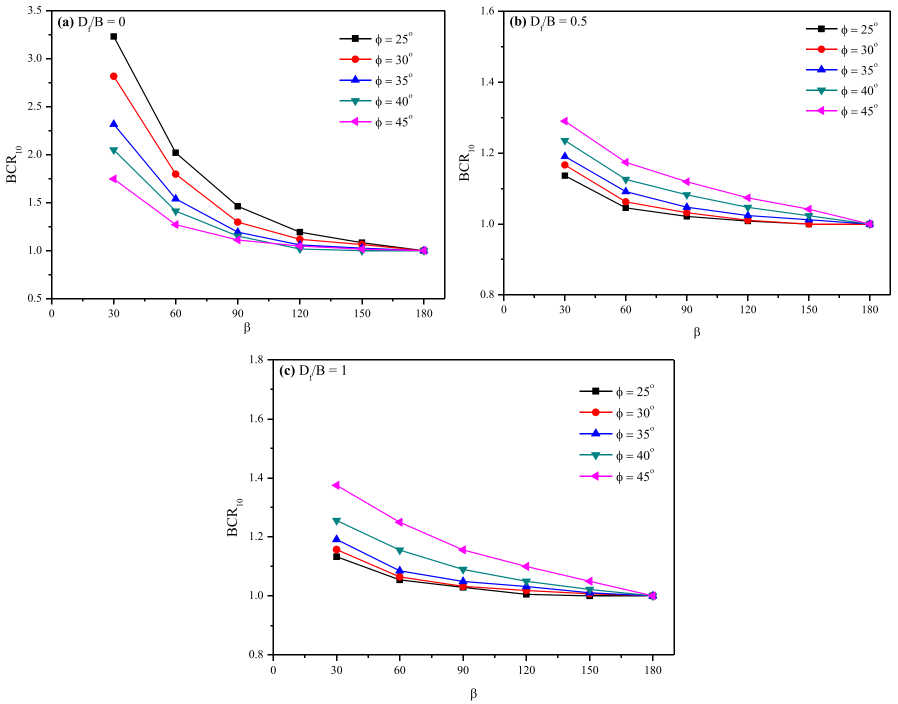

Fig. 5 Variation of bearing capacity ratio for different β and different ϕ at failure corresponding to S/D = 10% for **a** $D_f/B=0$, **b** $D_f/B=0.5$, **c** $D_f/B=1$

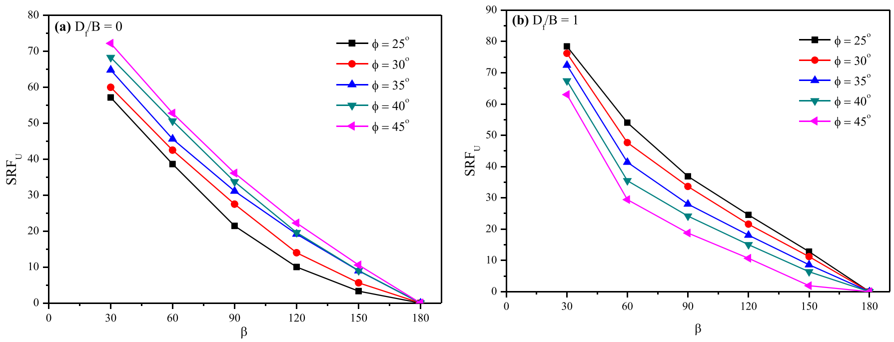

Fig. 6 Variation of settlement reduction factor with β at failure for different ϕ at **a** $D_f/B=0$, **b** $D_f/B=1$

placed on a surface with the highest friction angle of sand, i.e., ϕ = 45°. However, the SRF_u trends for an embedded footing ($D_f/D=1$) were in reverse order, with the SRF being greatest at the lowest friction angle. It follows that, in terms of settlement reduction, a conical foundation embedded at a given depth will be a viable option, particularly in soil with low shear strength. At $\beta=30°$, settlement reduction over circular footing is in the range of 60 to 80% considering all the friction angles and embedment ratios.

Figure 7a and b show the variation of SRF_{10} corresponding to S/D = 10% with β for different ϕ at $D_f/B = 0$ and 1, respectively. From the curves, it is observed that on increasing the β, SRF decreases which also means improvement in settlement reduction of conical footing decreases with increasing β. At $\beta = 30°$, the settlement reduction over circular footing is in the range of 55 to 75% considering all the friction angles and embedment ratios. The settlement reduction over circular footing is maximum for a lower value of friction angle. For a given value of β and ϕ, the SRF_{10} decreases with an increase in the embedment ratio. Furthermore, SRF_{10} values were marginally smaller than SRF_u.

4.4 Variation and Comparison of N_γ and N_q

From the ultimate bearing capacity obtained using the pressure settlement curve for a footing placed on a surface, the bearing capacity factor N_γ was estimated. Table 3 shows the comparison of N_γ values for conical footing placed on the sand obtained from the present study with Khatri and Kumar (2009). The present N_γ values nearly match the results of Khatri and Kumar (2009). Similarly, the present N_q variation is compared with the result obtained by Lyamin et al. (2007) for strip footing placed on the ground, as shown in Table 4. The result of the present study in terms of N_q is marginally less than those of Lyamin et al. (2007). The $N\gamma$ and N_q values obtained in the present study are smaller due to the use of the non-associated flow rule but comparable.

4.5 Variation and Comparison of s_γ and s_q

The bearing capacity of embedded conical footing can be expressed as:

$$q_{ult} = qN_q s_q d_q + 0.5\gamma B N_\gamma s_\gamma d_\gamma$$

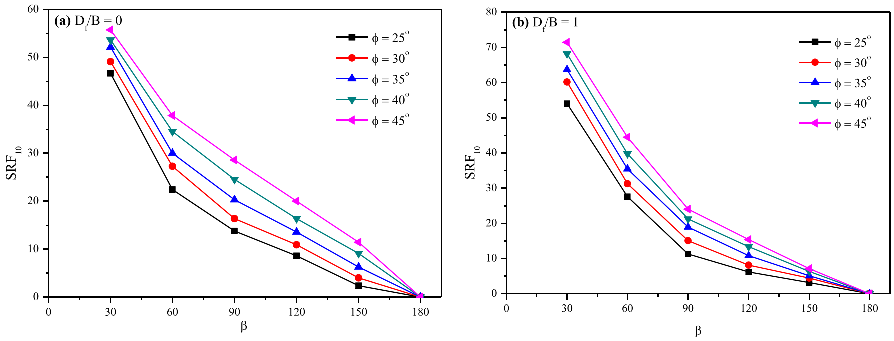

Fig. 7 Variation of settlement reduction factor for different β and different ϕ at failure corresponding to S/D = 10% for **a** $D_f/B = 0$, **b** $D_f/B = 1$

Table 3 Comparison of N_γ values for conical footing placed on the sand

Friction angle (ϕ)	N_γ values obtained from study						N_γ Khatri and Kumar (2009)					
	β = 30°	β = 60°	β = 90°	β = 120°	β = 150°	β = 180°	β = 30°	β = 60°	β = 90°	β = 120°	β = 150°	β = 180°
25°	37.7	12.5	7.48	6.46	6.34	4.64	41.53	14.57	8.55	6.88	6.1	5.68
30°	81.26	25.16	16.28	14.22	13.32	12.3	86.04	30.28	19.34	15.74	14.6	14.65
35°	175.12	60.46	37.08	33.14	31.34	35.22	189.07	68.62	45.82	38.92	37.2	36.97
40°	416.26	157.12	111.14	103.78	101.6	112.84	455.42	170.91	120.06	108.14	106.28	116.2
45°	1209.12	481.24	342.92	326.86	327.96	357.72	1225.4	490.33	364.72	341.24	343.44	379.79

Table 4 Comparison of N_q values for strip footing placed on the sand

Friction angle (ϕ)	Present N_q	Lyamin et al. (2007)
25°	8.10	10.66
30°	15.04	18.40
35°	27.20	33.3
40°	50.50	64.2
45°	115.30	134.87

In the above expression, the term s_q and s_γ take care of the plan shape of the footing, while d_q and d_γ relate to the increase of shear strength with depth which was not accounted for by Terzaghi (1943). The N_q and N_γ in the above equation correspond to the strip footing. Note that if the foundation is placed on a surface, the first term in the above expression related to the surcharge becomes zero. Furthermore, the depth factor d_γ in this study was taken as 1, consistent with Lyamin et al. (2007).

Hence, to determine the shape factor s_γ, the bearing capacity of conical footing placed on the surface was divided by the bearing capacity of surface strip footing. In this regard, an additional analysis was performed to determine the magnitude of N_γ of strip footing by keeping the width of strip footing (B) equal to the diameter of conical footing (B). Following the above, in the present study, the shape factor s_γ was computed for both circular and conical footing, and its variation with cone apex angle (β) was presented. Numerically, the shape factor can also be defined as

$$s_\gamma = \frac{(N_\gamma)_{\text{conical}}}{(N_\gamma)_{\text{strip}}} \tag{12}$$

The variation of s_γ with β and ϕ is shown in Table 5. From this table, it is worth noting that on increasing the apex angle of the cone, the s_γ value decreases, which means that on increasing β, the bearing capacity decreases for footing placed on the surface. Furthermore, the comparison of present s_γ for circular footing (β=180°) with Lyamin et al. (2007) is also shown in the same table. The current s_γ values for circular footing (β=180°) seem to almost match with Lyamin et al. (2007). From

Table 5 s_γ values calculated for conical footing

φ	β=30°	β=60°	β=90°	β=120°	β=150°	β=180°	β=180° Lyamin et al. (2007)
25°	4.54	2.14	1.42	1.24	1.15	1.01	0.96
30°	4.71	2.23	1.55	1.36	1.24	1.12	1.06
35°	4.77	2.27	1.70	1.45	1.36	1.27	1.2
40°	5.61	2.49	1.83	1.69	1.59	1.49	1.42
45°	6.69	2.86	2.17	2.00	1.93	1.79	1.7

Table 5, it can also be observed that the shape factor s_γ increases with an increase in friction angle (ϕ) for any given value of β.

The shape factor s_q corresponding to various embedment depths is calculated by taking a ratio of the difference in the bearing capacity of conical footing at a given embedment depth to the bearing capacity of the footing placed on a surface to the bearing capacity of strip foundation at the same embedment depth (Eq. 13). Numerically the expression of s_q is given as follows:

$$s_q = \left[\frac{q_b - (0.5 \times \mathrm{s}_\gamma \times \gamma \times \mathrm{B} \times N_\gamma)}{(d_q \times q \times N_q)}\right] \tag{13}$$

The term q_b refers to the bearing capacity of embedded conical footing, while the term 0.5 $s_\gamma B_\gamma N_\gamma$ relates to the bearing capacity of conical footing placed at the surface. The shape factor s_γ is defined in the previous section. The variation of s_q for the range of ϕ, D_f/B, and ϕ is depicted in Fig. 8a–f. From Fig. 8a–f, it has been observed that on s_q value decreases with an increase in apex angle and increases with a rise in friction angle. On increasing embedment depth for a particular value of friction angle, the s_q value increases. Accordingly, the bearing capacity also increases. The comparison of present s_q values with Lyamin et al. (2007) for circular footing (β = 180°) is indicated in Fig. 9. The current s_q values were slightly smaller but comparable with that reported by Lyamin et al. (2007) due to the use of the non-associated flow rule.

4.6 Variation and Comparison of d_q

In the bearing capacity equation, the N_γ term relates to the slip mechanism that develops beneath the footing's base. It means that the surcharge term, together with depth factor d_q captures the impacts of the portion of the mechanism that extends above the base of the footing. For determining d_q, the analysis was first performed by embedding the strip footing at different depths, and subsequently, the ultimate bearing capacity was computed using the pressure-settlement curve. Following this, the bearing capacity of the surface footing ($0.5B_\gamma N_\gamma$) was subtracted from the bearing capacity corresponding to the embedded footing. This difference in bearing capacity (qN_qd_q) is related to the component on account of surcharge due to shear strength above the foundation's base level. Accordingly, the depth factor d_q, which takes care of the shear strength above the foundation's base level, was determined by dividing the term qN_qd_q by the bearing capacity of surface strip footing subjected to surcharge, i.e., qNq.

Numerically d_q is defined as the depth factor calculated for different embedment depths at different φ by:

$$d_q = \left[\frac{q_{bstrip} - \left(0.5 \times B \times \gamma \times N_\gamma\right)}{(q \times N_q)}\right] \tag{14}$$

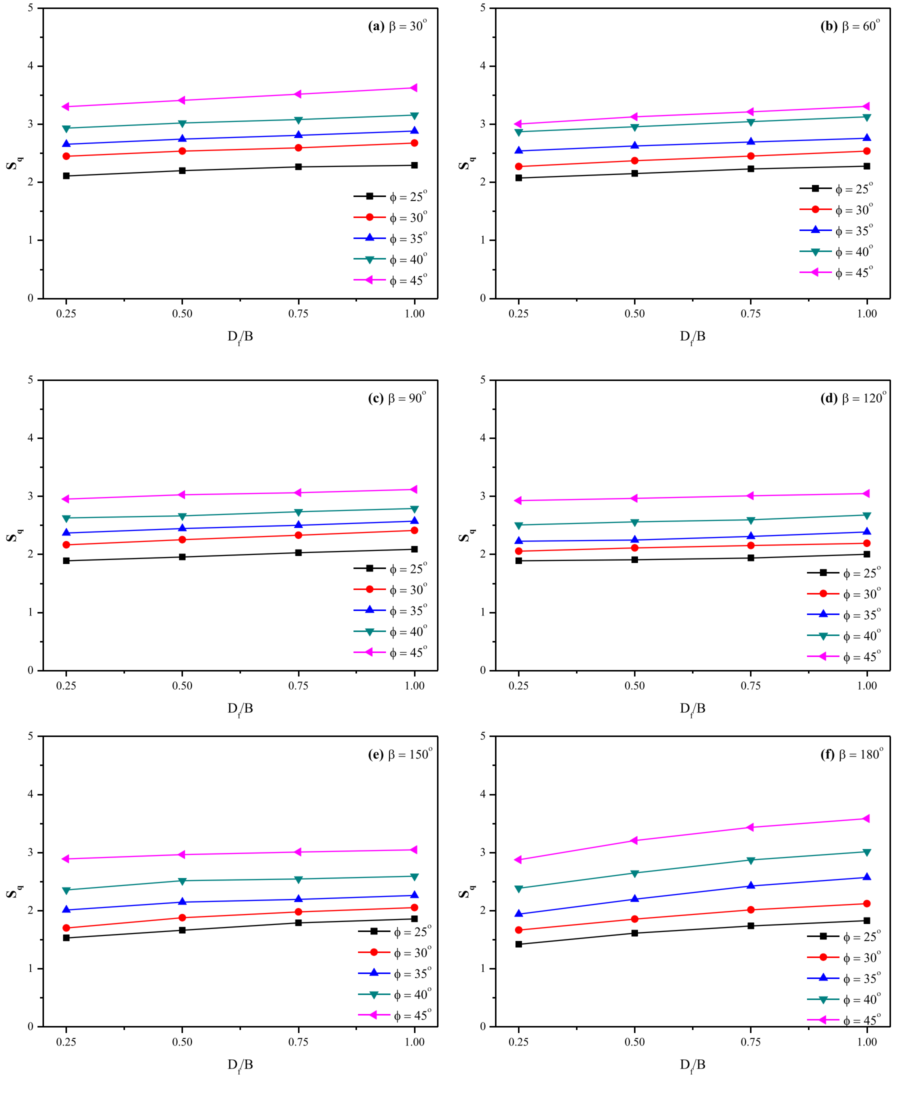

Fig. 8 Variation s_q vs D_f/B curves for different **ϕ** at β **a** 30°, **b** 60°, **c** 90°, **d** 120°, **e** 150°, and **f** 180°

where q_{bstrip} is the bearing capacity of the strip foundation at failure for different embedment depths, q is the surcharge ($_{\gamma}D_f$), and N_γ and N_q are the bearing capacity factors for strip footing resting on the ground.

The d_q values obtained as per the above-mentioned procedure were compared with those reported by Lyamin et al. (2007). This comparison is shown in Table 6, which suggests that the present d_q values were similar to that reported by Lyamin et al. (2007).

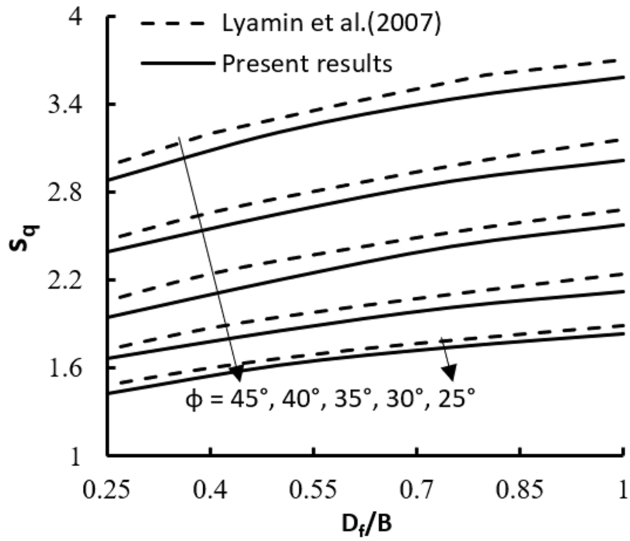

Fig. 9 Variation and comparison of S_q vs D_f/B with different ϕ for circular footing

Table 6 Comparison of d_q values for strip footing on homogeneous sand at various embedment depths

ϕ	D_f/B	d_q (present results)	d_q (Lyamin et al. 2007)
25°	0.25	1.69	1.71
	0.5	1.54	1.56
	0.75	1.51	1.51
	1	1.49	1.49
30°	0.25	1.70	1.73
	0.5	1.56	1.57
	0.75	1.52	1.52
	1	1.51	1.49
35°	0.25	1.72	1.73
	0.5	1.59	1.58
	0.75	1.53	1.52
	1	1.52	1.49
40°	0.25	1.76	1.78
	0.5	1.60	1.62
	0.75	1.54	1.55
	1	1.53	1.52
45°	0.25	1.81	1.84
	0.5	1.63	1.67
	0.75	1.57	1.60
	1	1.55	1.56

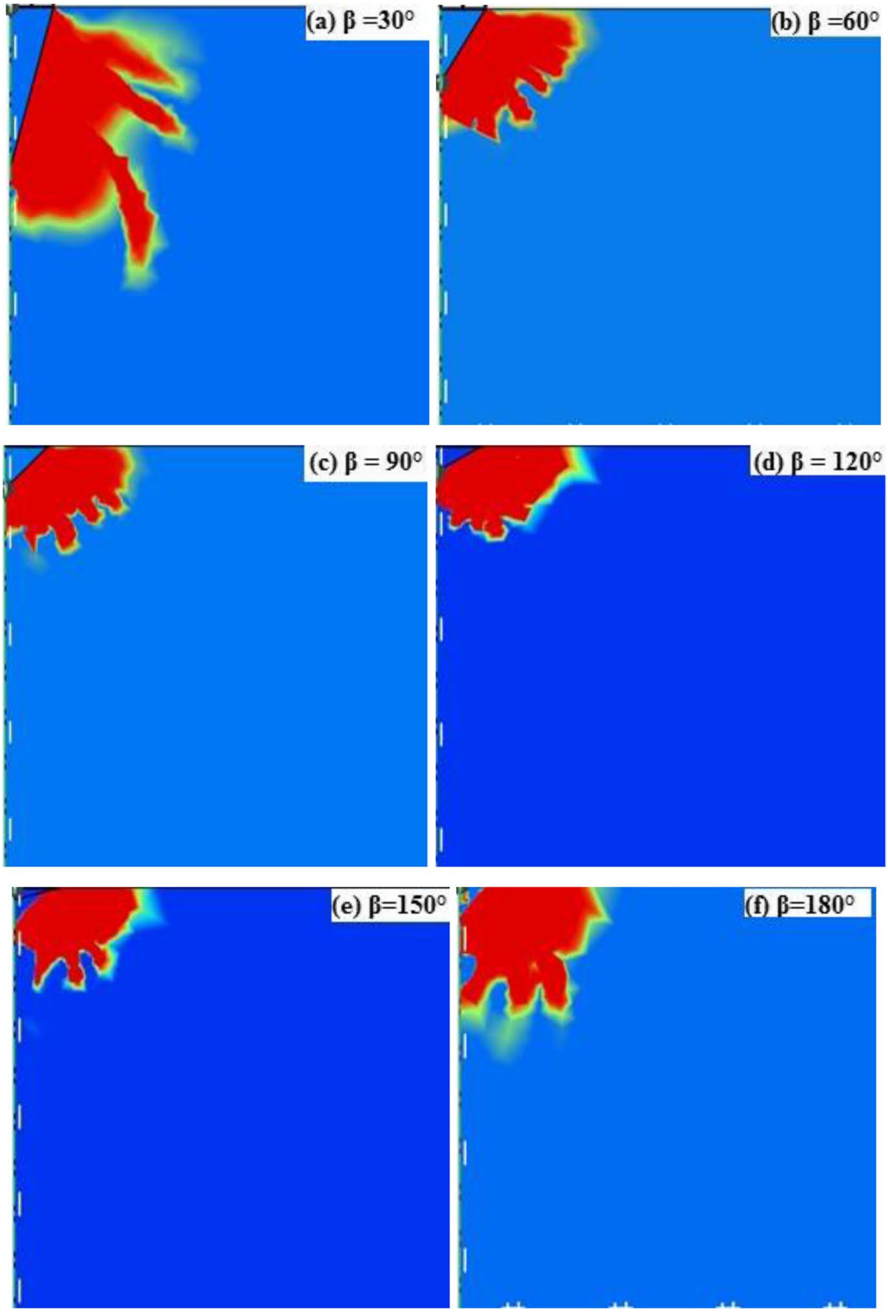

Fig. 10 Generated failure patterns for conical footing with $\phi = 35°$ and $D_f/B = 0$ at β a 30°, **b** 60°, **c** 90°, **d** 120°, **e** 150°, and **f** 180°

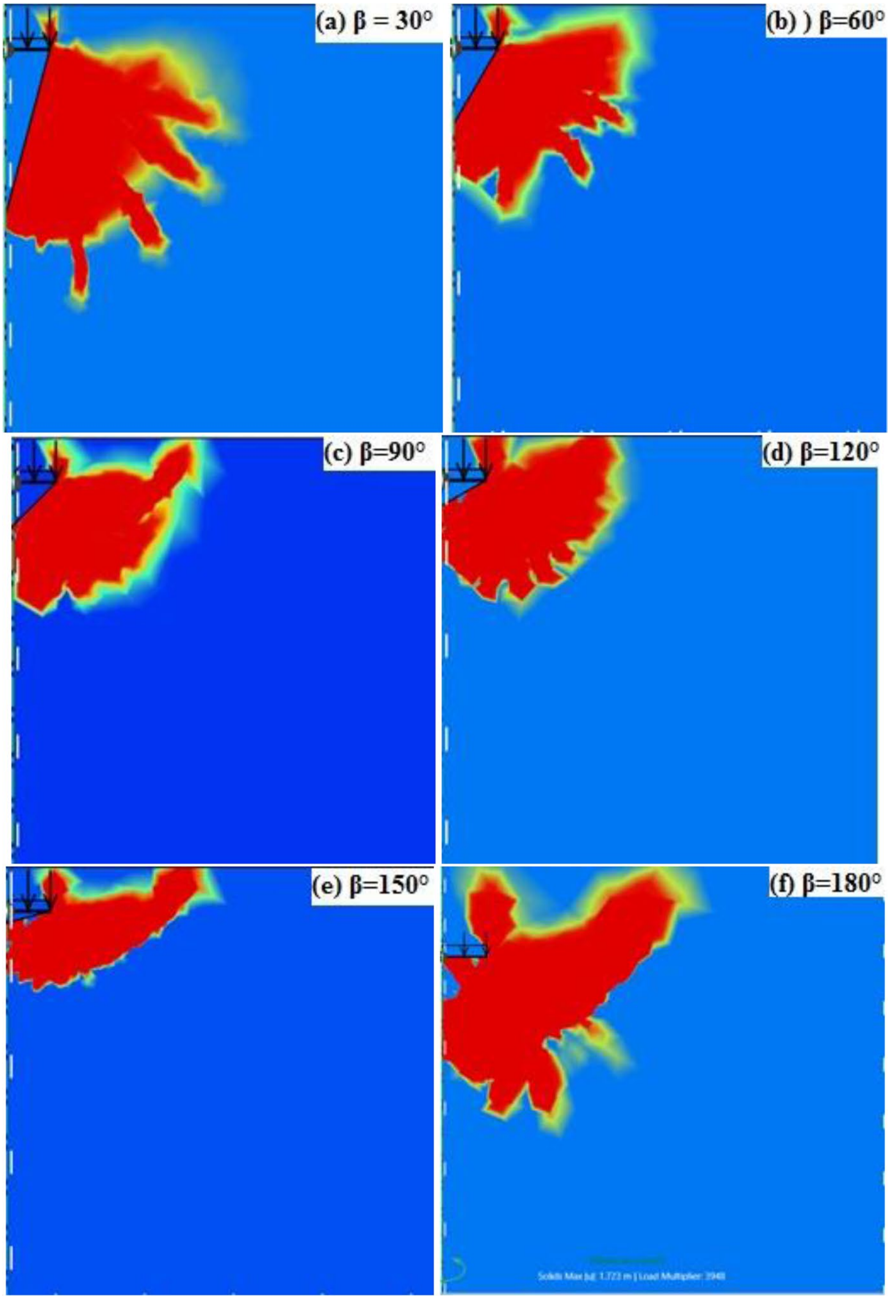

Fig. 11 Generated failure patterns for conical footing with $\phi = 35°$ and $D_f/B = 1$ at β **a** 30°, **b** 60°, **c** 90°, **d** 120°, **e** 150°, and **f** 180°

4.7 Failure Patterns

The generated failure patterns for conical footing with $\phi = 35°$ and $D_f/B = 0$ and 1 at $\beta = 30°$, 60°, 90°, 120°, 150°, and 180° are shown in Fig. 10a–f and Fig. 11a–f, respectively. The parameter indicated in Fig. 10a–f is the strain in the form of $|\varepsilon_{1,p} - \varepsilon_{3,p}|$. The dark red color in this figure implies the material is at failure. Alternatively, the adaptive finite element meshes shown in Fig. 2 indirectly reflect the failure patterns. The failure patterns generally serve two purposes: (1) to visualize the occurrence of failure and (2) to verify the correctness of the obtained results. It should also be noted that the curvilinear collapse pattern or rupture surface was always covered well within the stipulated vertical and horizontal range. It indicates that the analysis domain chosen was adequate. From the failure patterns, it can be seen that the failure surface is not well developed and is not reaching the ground. So, it can be concluded that there may be a possibility of local shear failure.

5 Conclusions

- Bearing capacity decreases on increasing the cone's apex angle (β), with the maximum at $\beta = 30°$.
- At $\beta = 30°$, bearing capacity improvement over circular footing was in the range of 1.25 to 5, considering all the friction angles and embedment ratios.
- At a given pressure, settlement increases on increasing the apex angle of the cone and becomes minimum at $\beta = 30°$.
- At $\beta = 30°$, settlement reduction over circular footing is in the range of 60% to 80%, considering all the friction angles and embedment ratios.
- The bearing capacity improvement and settlement reduction over circular footing are maximum for lower friction angle values.
- For a value of β and ϕ, the BCR decreases with an increase in the embedment ratio.
- The bearing capacity factors from the present study were marginally smaller than that reported in the literature, while the shape and depth factors were comparable. It implies that the flow rule only affected the bearing capacity factors but not the shape and depth factors.

Notations B: Diameter of the conical footing; ϕ: The angle of internal friction of sand; ψ: The angle of dilation of sand; E: Young's modulus of elasticity of sand; ν: Poisson's ratio of sand; Q: Vertically downward surcharge load acting on the footing; L: Length of the problem domain; V: Depth of the problem domain; u: Horizontal displacement; w: Vertical displacement; t: The thickness of the footing; c: Cohesion of soil; γ: Unit weight of sand; N_q: Bearing capacity factor; N_γ: Bearing capacity factor; q_0: Surcharge acting over the sand layer; q_b: Bearing capacity at failure; q_{10}: Bearing capacity at 10% settlement; D_f: Embedment depth from the surface; s_γ: Shape factor for surface; d_q: Depth factor for embedment depth; s_q: Shape factor for embedment depth; SRF: Settlement reduction factor; SRF_u: Settlement reduction factor at failure; SRF_{10}: Settlement reduction factor at the settlement of 10%; BCR: Bearing capacity ratio; BCR_u: Bearing capacity ratio at failure; BCR_{10}: Bearing capacity ratio at the settlement of 10

Author Contribution All authors contributed to the study conception and design. Material preparation, data collection, and analysis were performed by Ketan Shrivastava and Vishwas Nandkishor Khatri. The first draft of the manuscript was written by Jitendra Singh Yadav and all authors commented on previous versions of the manuscript. All authors read and approved the final manuscript.

Data Availability The datasets generated during and/or analyzed during the current study are available from the corresponding author on reasonable request.

Declarations

Ethics Approval and Consent to Participate Not applicable

Consent for Publication Not applicable.

Competing Interests The authors declare no competing interests.

References

Bowles, J.E.: Foundation analysis and design, By McGraw-Hill Book Companies. (1996).

Cassidy, M.J., Houlsby, G.T.: Vertical bearing capacity factors for conical footings on sand. Geotechnique **52**, 687–692 (2002). https://doi.org/10.1680/geot.2002.52.9.687

Chakraborty, M., Kumar, J.: Bearing capacity factors for a conical footing using lower-and upper-bound finite elements limit analysis. Can. Geotech. J. **52**, 2134–2140 (2015). https://doi.org/10.1139/cgj-2014-0507

Chakraborty, M., Kumar, J.: The size effect of a conical footing on Nγ. Comput. Geotech. **76**, 212–221 (2016). https://doi.org/10.1016/j.compgeo.2016.03.010

Das, P.P., Khatri, V.N., Doley, R., Dutta, R.K., Yadav, J.S.: Estimation of bearing capacity of shallow footings on layered sand using finite elements analysis. J. Eng. Des. Technol. (2022). https://doi.org/10.1108/JEDT-09-2021-0493

Houlsby, G.T., Martin, C.M.: Undrained bearing capacity factors for conical footings on clay. Géotechnique. **53**, 513–520 (2003). https://doi.org/10.1680/geot.53.5.513.37507

Hu, P., Leo, C., Liyanapathirana, S.: Horizontal bearing capacity factors for conical footings on clay. Appl. Ocean Res. **127**, 103308 (2022)

Keawsawasvong, S.: Bearing capacity of conical footings on clays considering combined effects of anisotropy and non-homogeneity. Ships and Offshore Structures. 1–12 (2021a). https://doi.org/10.1080/17445302.2021.1987110

Keawsawasvong, S.: Bearing capacity of conical footings on Hoek-Brown rock masses using finite element limit analysis. Int. J. Comput. Mater. Sci. Eng. **10**(03), 2150015 (2021b)

Khatri, V. N., Kumar, J.: bearing capacity factor Nγ for a rough conical footing. Geomech. Eng. **1**, (2009)

Khatri, V.N., Singh, N., Dutta, R.K., Yadav, J.S.: Numerical estimation of bearing capacity of shallow footings resting on layered sand. Transp. Infrastruct. Geotechnol. (2022). https://doi.org/10.1007/s40515-022-00236-4

Kumar, J., Khatri, V.N.: Bearing capacity factors of circular foundations for a general c– ϕ soil using lower bound finite elements limit analysis. Int. J. Numer. Anal. Methods Geomech. **35**, 393–405 (2011). https://doi.org/10.1002/nag

Lai, V.Q., Shiau, J., Van, C.N., Tran, H.D., and Keawsawasvong, S.: "Bearing capacity of conical footing on anisotropic and heterogeneous clays using FEA and ANN." Marine Georesour Geotechnol. 1–18 (2022)

Lyamin, A.V., Salgado, R., Sloan, S.W., Prezzi, M.: Two- and three-dimensional bearing capacity of footings in sand. Geotechnique **57**, 647–662 (2007). https://doi.org/10.1680/geot.2007.57.8.647

Optum G2. Finite element program for geotechnical analysis. (2019) https://optumce.com/

Phuor, T., Harahap, I.S., Ng, C.Y.: Bearing capacity factors for rough conical footing by viscoplasticity finite-element analysis. Int. J. Geomech. **22**(1), 04021266 (2022)

Potts, D.M., Zdravković, L., Addenbrooke, T.I., Higgins, K.G., Kovačević, N.: Finite element analysis in geotechnical engineering: application (Vol. 2), London: Thomas Telford (2001)

Terzaghi, K.: Theoretical soil mechanics. John Wiley and Sons Inc., New York 314 (1943)